

SLAC - PUB - 3484  
October 1984  
T/E

PARALLEL SCORES IN STOCHASTIC  
METHODS-APPLICATION TO COMPACT QED\*

D. DAHL AND R. BLANKENBECLER

*Stanford Linear Accelerator Center  
Stanford University, Stanford, California, 94305*

ABSTRACT

A new stochastic algorithm for calculating the properties of Hamiltonian lattice field theories is described. This approach improves the efficiency as well as the statistical accuracy of Projector Method simulations. As an example, this new method (called Parallel Scoring) is applied to PQED. Parallel Scoring is the software equivalent of parallel processing. Its advantages and disadvantages are illustrated and discussed. Numerical results from the application of the parallel processing algorithm to PQED in two space dimensions are presented and compared to earlier work.

Submitted to *Physical Review D*

---

\* Work supported by the Department of Energy, contract DE - AC03 - 76SF00515.

## 1. Introduction

For large  $\beta$ ,  $\exp(-\beta H)$  can be used to project onto the eigenstate of  $H$  with the minimum eigenvalue. For example, denoting this lowest value by  $E$ , we have

$$e^{-(\beta'-\beta)E} = \lim_{\beta', \beta \rightarrow \infty} \frac{\langle \chi | e^{-\beta' H} | \phi \rangle}{\langle \chi | e^{-\beta H} | \phi \rangle}, \quad (1)$$

if the corresponding eigenvector  $|\psi\rangle$  is not orthogonal to the trial states  $|\phi\rangle$  and  $|\chi\rangle$ . One also can evaluate the expectation value of an operator  $Q$  in the state  $|\psi\rangle$  by using

$$\langle \psi | Q | \psi \rangle = \lim_{\beta \rightarrow \infty} \frac{\langle \chi | e^{-\beta H} Q e^{-\beta H} | \phi \rangle}{\langle \chi | e^{-2\beta H} | \phi \rangle}. \quad (2)$$

Correlation functions can be computed in a similar way.

These equations form the starting point for the Projector Monte Carlo approach<sup>1</sup> which uses a stochastic method of evaluation introduced by Ulam and von Neumann,<sup>2</sup> and recently discussed by Kuti.<sup>3</sup> There are many possible schemes for implementing this approach, ranging from the population method pioneered by Kalos<sup>4</sup> and Ceperely and Adler,<sup>5</sup> to the modified projector method<sup>6</sup> to the approach of Ref. 1.

In this paper we shall discuss a new variant of the stochastic approach which seems to offer both a reduction of statistical fluctuations and an increase in efficiency by being able to compute several matrix elements of the problem simultaneously. These matrix elements may even be in orthogonal sectors. We term this new scoring method *Parallel Scores*, and shall illustrate its use and effectiveness by applying it to compact QED<sup>7</sup> in two space dimensions.<sup>8</sup> Three dimensions will be discussed in a subsequent paper.

## 2. Parallel Scores

In order to implement the stochastic method, the projection operator in Eq. (1) usually must be simplified. The first step is to subdivide  $\beta$  into  $L$  subintervals of width  $\Delta T = \beta/L$ :

$$e^{-\beta H} = \left( e^{-\Delta T H} \right)^L = (U(\Delta t))^L . \quad (3)$$

It is normally necessary to go one step further and to break the Hamiltonian  $H$  in  $U$  into  $H_1$  and  $H_2$ , or  $U = U(2)U(1)$ , such that the matrix elements of  $U(k)$  are easy to evaluate. By breaking the lattice up into independent subelements (e.g. the checkerboard breakup described in Ref. 1 and Ref. 7) this simplification can be achieved.

The sum over intermediate states implicit in Eq. (3) is evaluated stochastically with importance sampling. We write

$$\langle i | U(\Delta T, k) | j \rangle = S_{ij}(\Delta T, k) P_{ij}(k) , \quad (4)$$

where  $S_{ij}$  is the score, and  $P_{ij}$  the probability, which satisfies

$$\sum_i P_{ij}(k) = 1 . \quad (5)$$

The precise form for the probabilities is not fixed by the above and they can be chosen to minimize the fluctuations in the final measured quantity of interest, in part by “smoothing” out the breakup into  $U(2)U(1)$  (see Ref. 1 and 6) and in part by narrowing the distribution of final scores.

Using the probabilities  $P_{ij}$  to generate a trip through the intermediate states, the corresponding weight of this contribution is then the product of each of the corresponding elemental scores,

$$W(L, \Delta T) = \prod_1^L S(\Delta T) . \quad (6)$$

By averaging over many such paths denoted by  $\langle \rangle$ , one achieves an estimate of, for example,

$$\langle \chi | \exp(-\beta H) | \phi \rangle = \langle W(L, \Delta T) \rangle . \quad (7)$$

#### ENERGIES:

In previous applications of the projector method, the energy of Eq. (1) was evaluated by the standard method of dividing the internal  $\beta'$  into  $L + \Delta L$  intervals, and then going  $\Delta L$  extra steps in evaluating the numerator  $N$  as compared to the denominator  $D$ . However there is a more efficient way to proceed.

In this, the simplest application of the *parallel score* idea, one goes  $L$  steps for both  $N$  and  $D$ , but uses different scores. Define  $\beta = L\Delta T$ ,  $\beta' = L\Delta T'$ , and

$$S_{ij}(\Delta T, k) \equiv \langle i | U(\Delta T, k) | j \rangle / P_{ij}(k) \quad (8)$$

$$S_{ij}(\Delta T', k) \equiv \langle i | U(\Delta T', k) | j \rangle / P_{ij}(k) .$$

By using the *same* probabilities, the configuration generated by  $P_{ij}$  can be used to evaluate both  $N$  and  $D$  so that

$$\exp(-L(\Delta T' - \Delta T)E) = \frac{\langle W(L, \Delta T') \rangle}{\langle W(L, \Delta T) \rangle} . \quad (9)$$

We find that choosing  $\Delta T'$  to be from 1% to 10% different from  $\Delta T$  is satisfactory and has no effect on the extracted energy value. This algorithm is not only more

efficient than the standard method, but we find that the fluctuations are smaller due to cancellations in the ratio present in Eq. (9). Numerical examples will be given later that demonstrates these features.

### *ENERGY GAPS:*

One is often interested in computing the energy gaps between orthogonal sectors of a model. In the later application to PQED, we will want to calculate the string tension. Thus the energy of states of the model with strings of differing lengths must be computed. It is, of course, possible to simply use the previous method for differing choices of the initial state  $|\phi\rangle$  and then to subtract the resultant energies. However, as we shall see, parallel scoring allows all string lengths (and positions) to be run simultaneously. As an additional benefit we again find an improvement in statistical accuracy is possible because the correlated fluctuations in the energy values of the different sectors allows one to cancel the major part of the statistical error in the extracted energy gaps.

Since most of the computer time is spent in generating the random lattice configurations, and little time is spent keeping score, this algorithm is much more efficient. It is in this sense that parallel scoring is the software equivalent of parallel hardware.

Although this application of parallel scoring cannot be applied to all models, it is possible to discuss this scheme in a quite general context. We shall use the example and language of PQED in order to make the exposition more understandable. In the charge-free sector of the theory, the vacuum properties are computed by generating a sequence of configurations such that the matrix element between two consecutive states  $j_0 \rightarrow i_0$  is related to the score and prob-

ability by

$$\langle i_0 | U | j_0 \rangle = S_{i_0 j_0} P_{i_0 j_0} . \quad (10)$$

The crucial point is now to note that in the string sector there is a corresponding matrix element.

$$\langle i_1 | U | j_1 \rangle = S_{i_1 j_1} P_{i_1 j_1} . \quad (11)$$

It is obtained by a unique mapping of  $i_0 \rightarrow i_1$  and  $j_0 \rightarrow j_1$ , which is constructed by incrementing the value of the electric flux quantum numbers on those links that are included in the string. For a given positioning of the string, this mapping is unique. For fixed external changes, there are many suitable interpolating string configurations. Our final answer would be independent of this choice (for large  $\beta$ ).

In the case of PQED (in which any number of flux units can be added by the operator  $U$  to a link) note first that  $P_{i_0 j_0}$  is nonzero whenever  $P_{i_1 j_1}$  is nonzero. This circumstance suggests the following algorithm: use  $P_{i_0 j_0}$  to generate the random lattice configuration and use this in evaluating the score for both the vacuum and the string sector. Note that in traversing the lattice in these different sectors, the corresponding single plaquette matrix elements (and scores) differ only when the suggested flux change is in a plaquette that is adjacent to the string. In this case we increment the string score by  $S_{i_0 j_0} \cdot \Delta S_{i_0 j_0}$  where

$$\Delta S_{i_0, j_0} = \frac{\langle i_1 | U | j_1 \rangle}{\langle i_0 | U | j_0 \rangle} . \quad (12)$$

$\Delta S$  compensates for the fact that we have used the vacuum probability and that we have extracted the vacuum part of the score. One can either compute and

store a special table for  $\Delta S$  or compute it from the standard vacuum score and probability table.

The implementation of this algorithm proceeds by marching through the lattice, making moves according to the vacuum link configurations and accumulating the scores. When the visited plaquette is next to the string, one accumulates  $\Delta S$ . At the end of the run, there are two types of scores, one for the vacuum and a partial one for the string:

$$W(L, \Delta T) = \Pi S(\Delta T) \quad \Delta W(K, \Delta T) = \Pi \Delta S(\Delta T) . \quad (13)$$

The corresponding average weights give the estimated matrix element for the vacuum and the string:

$$\langle W | e^{-\beta H} | \phi_0 \rangle = \langle W \rangle \quad \text{and} \quad \langle \chi | e^{-\beta H} | \phi_1 \rangle = \langle W \cdot \Delta W \rangle . \quad (14)$$

The energies can now be calculated separately by using the Parallel Score Method of Eq. (8) but it is more accurate (because the fluctuations are strongly correlated) to compute the gaps directly for each string length,

$$e^{-L \cdot \Delta T (E_1 - E_0)} = \frac{\langle W(L, \Delta T) \Delta W(L, \Delta T) \rangle}{\langle W(L, \Delta T) \rangle} . \quad (15)$$

or to compute directly the difference in energies due to the addition of extra links to the length of the string. Thus the process of generating the basic configuration is independent of the presence or absence of a string of any length. Hence, from this basic configuration, which is that of the vacuum, we can simultaneously generate extra score factors reflecting the presence of a string of varying lengths and positions. In fact, we can accumulate  $\Delta W$  for each plaquette as though it

were adjacent to the string. One can then compute the full  $\Delta W$  for many possible string lengths and positions on the lattice, thereby improving the statistical accuracy with little additional cost.

### 3. Periodic Quantum Electrodynamics

We apply the general ideas developed above to a specific example: Periodic Quantum Electrodynamics in two spatial dimensions. After decomposing the Hamiltonian we analyze the single plaquette matrix elements. With these building blocks we demonstrate the substantial increase in numerical accuracy which results from the parallel score and trial parameter techniques (see next section).

Our Hamiltonian is

$$H = g^2 \sum_{\ell} E_{\ell}^2 - \frac{1}{g^2} \sum_p \cos B_p$$

$$B_p = A_{\ell_1} + A_{\ell_2} - A_{\ell_3} - A_{\ell_4} \quad (16)$$

$$[E_{\ell}, A_j] = \frac{1}{i} \delta_{j\ell}.$$

Of course,  $\ell_1, \dots, \ell_4$  are the four links bordering plaquette  $p$ . The components of the electric field and vector potential are canonically conjugate operators associated to each link of a finite lattice with toroidal boundary conditions. The basis in Hilbert space is specified by simultaneously diagonalizing the electric field operators:

$$E_{\ell} |n\rangle = n_{\ell} |n\rangle \quad n_{\ell} = 0, \pm 1, \pm 2, \dots \quad (17)$$

Residual gauge symmetries allow us to label the sectors of Hilbert space according to the background electric charge. Our choice of basis is compatible with this labelling of sectors.

The purpose of decomposing the Hamiltonian is to reduce all computations of the matrix elements of  $U$  to a purely local problem. The following decomposition achieves this goal:

$$H = H_1 + H_2$$

$$H_k = \frac{1}{2} g^2 \sum_{\ell} E_{\ell}^2 - \frac{1}{g^2} \sum_{p \in \mathcal{P}_k} \cos B_p \quad k = 1, 2. \quad (18)$$

Here  $\mathcal{P}_k$  partitions the set  $\mathcal{P}$  of all plaquettes in the lattice into two disjoint subsets whose union gives  $\mathcal{P}$ . The sum over  $\ell$  is over all links of the lattice. This partition forms the usual checkerboard.

In order to implement the ideas of the earlier sections we need to compute matrix elements of the exponentiated sub-Hamiltonians. This becomes easy once we note that

$$H_k = \sum_{p \in \mathcal{P}_k} h_p$$

$$h_p = \frac{g^2}{2} (E_{\ell_1}^2 + E_{\ell_2}^2 + E_{\ell_3}^2 + E_{\ell_4}^2) - \frac{1}{g^2} \cos B_p \quad (19)$$

$$[h_p, h_q] = 0 \quad \Leftarrow (p \in \mathcal{P}_k \Rightarrow q \in \mathcal{P}_k).$$

Note that each plaquette Hamiltonian contains all four electric field operators weighted by a factor of  $1/2$  to avoid double counting.

Now that each  $H_k$  has been expressed as a sum of commuting operators, exponentiation is easy:

$$e^{-\Delta H_k} = \prod_{p \in \mathcal{P}_k} e^{-\Delta h_p}, \quad (20)$$

where  $\Delta$  is either  $\Delta T$  or  $\Delta T'$ . Matrix elements of  $e^{-\Delta H_k}$  are then products of single plaquette matrix elements. We now focus our attention on these.

The following combinations of operators simplify the treatment of the single plaquette Hamiltonian:

$$\begin{aligned}
m_0 &\equiv E_1 - E_2 - E_3 - E_4 \\
m_1 &\equiv E_1 + E_2 + E_3 + E_4 \\
m_2 &\equiv E_1 - E_2 + E_3 - E_4 \\
m_3 &\equiv E_1 - E_2 - E_3 + E_4 .
\end{aligned} \tag{21}$$

This is an orthogonal Walsh transform on the electric field operators, and satisfies

$$4 \sum_{i=1}^4 E_i^2 = \vec{m}^2 + m_0^2 . \tag{22}$$

The vector components of  $m$  commute with  $h$  and each other:

$$[h, \vec{m}] = [m_i, m_j] = 0 \quad i, j = 1, 2, 3 . \tag{23}$$

Our single plaquette basis states are eigenstates of both  $n_1, \dots, n_4$  and  $\vec{m}, m_0$ , and we will use these labels interchangeably. Application of the Hamiltonian  $h$  to a basis state will then only change the quantum number  $m_0$ . Clearly the same statement applies to matrix elements of  $e^{-\Delta h}$ .

To obtain numerical values of the non-vanishing matrix elements we define

$$\begin{aligned}
h &= e + b \\
e &= \frac{g^2}{2} (E_1^2 + E_2^2 + E_3^2 + E_4^2) \\
b &= -\frac{1}{g^2} \cos(A_1 + A_2 - A_3 - A_4) .
\end{aligned} \tag{24}$$

and then approximate the exponential operator by choosing a finite value for  $s$

in the Trotter Product Formula:

$$\langle n'_i | e^{-\Delta h} | n_i \rangle \cong \langle n'_i | \left( e^{-(\Delta/2s)a} e^{-(\Delta/s)b} e^{-(\Delta/2s)c} \right)^s | n_i \rangle . \quad (25)$$

To evaluate the right hand side, we insert complete sets of states between each operator factor. The resulting matrix elements can be evaluated analytically and then the matrix multiplication can be carried out explicitly and easily by the computer.

The electric matrix elements are diagonal:

$$\langle n'_i | e^{-(\Delta/s)c} | n_i \rangle = \delta_{\bar{m}', \bar{m}} \delta_{m'_0, m_0} \exp \left( -\frac{\Delta}{4s} (\bar{m}^2 + m_0^2) \right) . \quad (26)$$

For the magnetic matrix element we use a function space realization:

$$\begin{aligned} \langle n'_i | e^{-(\Delta/s)b} | n_i \rangle &= \int_0^{2\pi} d\theta_1 \dots d\theta_4 \left( \frac{1}{2\pi} \right)^4 \exp \left[ -i \sum_{j=1}^4 (n'_i - n_i) \theta_j \right] \\ &\times \exp \left[ (\Delta/sg^2) \cos(\theta_1 + \theta_2 - \theta_3 - \theta_4) \right] \\ &= I_{|n'_i - n_i|} (\Delta/sg^2) \cdot \delta_{n_2 - n'_2, n_1 - n'_1} \delta_{-n_3 + n'_3, n_1 - n'_1} \delta_{-n_4 + n'_4, n_1 - n'_1} \\ &= I_{|(m'_0 - m_0)/4|} (\Delta/sg^2) \cdot \delta_{\bar{m}', \bar{m}} . \end{aligned} \quad (27)$$

To establish this result use the following generating function for the modified Bessel function:

$$e^{z \cos \theta} = I_0(z) + 2 \sum_{k=1}^{\infty} I_k(z) \cos(k\theta) . \quad (28)$$

Evaluation of the matrix elements of the exponentiated single plaquette

Hamiltonian proceeds by first combining the electric and magnetic matrix elements

$$\langle n_i' | e^{-(\Delta/2s)c} e^{-(\Delta/s)b} e^{-(\Delta/2s)c} | n_i \rangle = \delta_{\vec{m}', \vec{m}} E_s(\vec{m}) I_1(m_0', m_0), \quad (29)$$

where

$$E_s(\vec{m}) \equiv \exp\left(-\frac{\Delta g^2}{8s} \vec{m}^2\right)$$

$$I_1(m_0', m_0) \equiv e^{-(\Delta g^2/16s)(m_0'^2 + m_0^2)} I_{|m_0' - m_0/4|}(\Delta/s g^2)$$

and then raising this matrix to the  $s^{\text{th}}$  power:

$$\langle n_i' | \left( e^{-(\Delta/2s)c} e^{-(\Delta/s)b} e^{-(\Delta/2s)c} \right)^s | n_i \rangle = \delta_{\vec{m}', \vec{m}} \cdot E(\vec{m}) \cdot I(m_0', m_0)$$

where

$$E(\vec{m}) \equiv (E_s(\vec{m}))^s = \exp\left(-\frac{\Delta g^2}{8} \vec{m}^2\right) \quad (30)$$

$$I(m_0', m_0) \equiv I_s(m_0', m_0).$$

and

$$I_{s'}(m_0', m_0) \equiv \sum_{\vec{m}_0} I_{s'-1}(m_0', \vec{m}_0) I_1(\vec{m}_0, m_0), \quad s' = 2, \dots, s$$

$$\text{or} \quad I_{2s}(m_0', m_0) \equiv \sum_{\vec{m}_0} I_s(m_0', \vec{m}_0) I_s(\vec{m}_0, m_0).$$

It is worth noting that symmetries of the single plaquette Hamiltonian reduce considerably the storage requirements on the computer. Without special symmetries, one would need to store a single matrix element for each  $|n_i\rangle$  and  $|n_i'\rangle$ . Since each of these eight quantum numbers might assume up to ten values

(a conservative estimate), it would be necessary to store  $10^8$  matrix elements. The single plaquette symmetries mean that we can factor the typical matrix element into two parts, the first of which has simple functional dependence on all  $n_i$  and  $n'_i$  and the second of which has a complicated functional dependence on a small subset of quantum numbers. The complicated functional dependence is isolated to the two combinations of quantum number  $m_0$  and  $m'_0$  which occur in  $I_s$ . It is this factor which is computed during program initialization. The storage requirements are quite modest.

As a check on the accuracy of our approximations for the single plaquette problem we can evaluate the above matrix element with  $e = 0$ . The accuracy of computing the matrix element of  $e^{-\Delta h}$  will always be better than the accuracy of computing the modified matrix element of  $e^{-\Delta b}$ . That is because the terms truncated from the sum are highly damped by the presence of the factor  $e^{-\Delta e}$ . Analytic evaluation of the matrix element of  $e^{-\Delta b}$  gives a simple modified Bessel function. With  $s = 8$  and the intermediate state sum truncated to five states the accuracy is better than one part in a million. Thus we have solved the single plaquette problem (essentially) exactly for the matrix elements of interest.

#### 4. Implementation

As noted earlier, the choice of probabilities dictates the scores via (4). We will choose a form for our probabilities which solves the single plaquette problem exactly and augment it by adding two adjustable degrees of freedom.

In marching through the lattice, we come to a plaquette with quantum numbers  $\bar{m}, m_0$ . The probability for changing the quantum numbers to  $\bar{m}', m'_0$  can

be taken to be

$$\begin{aligned}
P_{\bar{m}, m_0 \rightarrow \bar{m}', m'_0} &\equiv \frac{\langle \bar{m}', m_0 | e^{-\Delta h} | \bar{m}, m_0 \rangle}{\sum_{\bar{m}'', m''_0} \langle \bar{m}'', m''_0 | e^{-\Delta h} | \bar{m}, m_0 \rangle} \\
&= \delta_{\bar{m}', \bar{m}} \frac{I(m'_0, m_0)}{\sum_{m''_0} I(m''_0, m_0)}.
\end{aligned} \tag{31}$$

From (4), the score associated with this transition is

$$\begin{aligned}
S_{\bar{m}, m_0 \rightarrow \bar{m}', m'_0} &= \sum_{\bar{m}'', m''_0} \langle \bar{m}'', m''_0 | e^{-\Delta h} | \bar{m}, m_0 \rangle \\
&= E(\bar{m}) \sum_{m''_0} I(m''_0, m_0).
\end{aligned} \tag{32}$$

This score enjoys the unique property that it is a constant independent of the final state. It is in this sense that the above form of the probabilities is an exact solution of the single plaquette problem. The constancy of the score implies that the average weight will give the exact matrix element with no fluctuations. For more than one coupled plaquette, this is no longer true, of course.

Reference to Eq. (30) shows that  $I$  is a function of  $\Delta$  and  $g^2$ . It is through this functional dependence that we will introduce the two additional degrees of freedom into the probabilities. The actual probability we use is given by

$$P_{\bar{m}, m_0 \rightarrow \bar{m}', m'_0} = \delta_{\bar{m}', \bar{m}} \frac{I(m'_0, m_0; g_T, \Delta_T)}{\sum_{m''_0} I(m''_0, m_0; g_T, \Delta_T)} \tag{33}$$

where  $I$  is computed from (30) with  $g$  and  $\Delta$  replaced by  $g_T$  and  $\Delta_T$ . The resultant score is

$$S_{\bar{m}, m_0 \rightarrow \bar{m}', m'_0} = E(\bar{m}) \frac{I(m'_0, m_0; g, \Delta)}{I(m'_0, m_0; g_T, \Delta_T)} \sum_{m''_0} I(m''_0, m_0; g_T, \Delta_T). \tag{34}$$

Now the score is no longer independent of the final quantum numbers.

The breakup of the Hamiltonian ,Eq. (18), furnishes an immediate reason for the introduction of trial parameters. Our breakup splits the electric term from each link evenly into  $H_1$  and  $H_2$ , thus introducing a factor of  $1/2$  in the electric part of the single plaquette Hamiltonian as compared to the magnetic term. To compensate for this factor and to achieve the correct electric suppression one can take  $g_T \cong \sqrt{2}g$ . The introduction of the second trial parameter  $\Delta_T$  will allow us to adjust the probability of adding flux to the system so as to minimize the final fluctuations.

We now show how the general description of parallel scoring given above translates into a simple specific algorithm. First address the parallel scoring method of obtaining energies. Typically one takes  $|\phi\rangle$  to be the strong coupling vacuum state, so that

$$E_\ell |\phi\rangle = 0 \tag{35}$$

for every link  $\ell$ . One begins marching through the lattice visiting first the plaquettes in  $\mathcal{P}_1$  then  $\mathcal{P}_2$ , and repeats this process  $L$  times. As each plaquette is visited in turn, its initial quantum numbers  $\vec{m}, m_0$  determine the probability for making a transition to final quantum numbers  $\vec{m}', m'_0$  via (33). Since the probabilities contain the factor  $\delta_{\vec{m}, \vec{m}'}$ , one need only choose amongst the final values of  $m'_0$ , and the probabilities for these final values are stored as an array indexed by  $m_0$  and  $m'_0$ . For a given  $m_0$ , the transition with the largest probability is usually  $m'_0 = m_0$ , and there is a preference to move towards  $m'_0 = 0$ . This bias stabilizes the random walk, a crucial feature for any set of acceptable probabilities (see point 4 in conclusions).

In both the naive and parallel score methods, one always includes at least

one score factor for each transition. This is given by (34). The part of the score which depends in a complicated way on  $m_0', m_0$  is stored as a two index array. The factors arising from  $\vec{m}$  are kept track of separately. The only modification arising in the Parallel Score method for energies is that a second similar score is also accumulated; from (7) and (33) we have the following form for this latter score,

$$S'_{\vec{m}, m_0 \rightarrow \vec{m}', m_0'} \equiv E(\vec{m}, \Delta T') \cdot \frac{I(m_0', m_0; g, \Delta')}{I(m_0', m_0; g_T, \Delta_T)} \quad (36)$$

$$\times \sum_{m_0''} I(m_0'', m_0; g_T, \Delta_T) .$$

It, too, is stored and referenced as a two-index array. If we denote the product of the  $S$  ( $S'$ ) over all plaquettes occurring in the  $L$  passes through the lattice by  $W(L, \Delta T)$  ( $W(L, \Delta T')$ ) then the energy is computed from (8).

All energies mentioned later in the paper will be computed from a pair of scores as explained above. We will not refer to both scores  $S$  and  $S'$  explicitly, but expect the reader to realize that this parallel scoring overlays the structure outlined next.

As discussed above, computation of string energies can be carried out simultaneously with the computation of vacuum sector energies. As in the simultaneous computation of numerator and denominator, this new application of parallel scores requires the accumulation of several additional scores while the usual algorithm generating the vacuum configurations proceeds as normal. The string energies are then directly given in terms of these additional scores.

To see the structure of one of these additional scores, consider the example of a string of unit length on link  $\ell$ . First, observe that matrix elements corresponding

to single plaquette transitions occurring at plaquettes not adjacent to the string do not change under the unique mapping from the vacuum sector to the string sector. Thus, the additional score factor can arise only from the transitions at the two plaquettes adjacent to the string. We will introduce an additional score factor  $\Delta S$  such that the expectation of its product with the vacuum score  $S$  yields the string sector matrix element (see Eq. (12)). From this criteria we can see that  $\Delta S$  is the product of the additional score factors for each of the two adjacent plaquettes;  $\Delta S = \Delta S_- \Delta S_+$ , where

$$\Delta S_{\pm} = \frac{E(\vec{m}_{\pm})}{E(\vec{m})} \cdot \frac{I(m'_{0\pm}, m_{0\pm}; g, \Delta)}{I(m'_0, m_0; g, \Delta)}. \quad (37)$$

The  $\pm$  indicates that  $m_0$  and  $m'_0$  are to be incremented or decremented by 1 depending on whether the unit of flux contributed by the string at link  $\ell$  changes the  $m_0$  quantum number in a positive or negative way. Thus if the string is one unit of right-pointing flux,  $\Delta S_+$  ( $\Delta S_-$ ) refers to an additional score for the plaquette below (above) the string.

For a string longer than one link, a straightforward extension of this algorithm will give the desired matrix element. The computer must form  $\Delta S_+$  or  $\Delta S_-$  for each plaquette bordering the string. The final additional score factor is then the product of all the  $\Delta S_+$  and  $\Delta S_-$ .

Until now, we have discussed simultaneous parallel scoring of the vacuum sector and a single string. There is no difficulty in keeping track of scores for many different positions of the two external charges at the same time. These different external charge sectors correspond to strings with varying lengths and positions. Thus, completion of a single  $L$ -step guided walk through the intermediate basis states will determine contributions to matrix elements for many string

configurations. Reduction of statistical fluctuations via position averaging of a given string size is possible in this single walk. Even without position averaging, computational time is reduced by a factor of  $\sim N$ , if one wishes to compute energies in  $N$  orthogonal charge sectors.

Of course, the score  $\Delta S$  is accompanied by  $\Delta S'$  as in (37). This is the requirement of the parallel score technique that allows one to sidestep the necessity of calculating the numerator and denominator of (1) with different  $L$  values. This structure exists side by side with the structure for working in orthogonal sectors simultaneously.

## 5. Numerical Results

The simplest measurement to make is that of the ground state energy density (energy per plaquette), given in Figure 1 as a function of coupling in the crossover region. Figure 2 shows similar numerical results for the  $8 \times 8$  lattice. The statistical fluctuations are slightly larger for the larger system.

In Figure 3, a comparison with standard strong coupling perturbation theory calculation is given, where the energy density is given by

$$E_o = -(2g^2)^{-3}(1 - 0.308(2g^2)^{-4} + \dots), \quad (38)$$

The curve in the figure was computed<sup>10</sup> including terms up to order  $g^{-32}$ . The strong coupling curve is not extended to small  $g$  since in this region the higher order terms in the series expansion become important. A few points from the variational calculation of Heys and Stump<sup>11</sup> are also shown in the same figure. Comparison amongst all three is excellent throughout the range of coupling in

which the strong coupling expansion is reliable. Our numerical results for the ground state energy are consistent with the upper bound given by Hofsäss and Horsley.<sup>12</sup>

Next we compare different methods of computing the energy density and gaps. The first method is operationally identical with the approach used by Potvin and DeGrand(Ref.7), but the probabilities and scores used were different, in ways that will be discussed in detail in the next section. A demonstration of the reduction in statistical fluctuations resulting from the use of parallel scoring is shown in Figure 4 . Method A computes the energies by the original method of going extra steps in the numerator as compared to the denominator, while both are evaluated using the same scores and probabilities. Method B, which provides the most basic and simplest application of parallel scoring, has been discussed above. In this method, the number of time steps is the same in the numerator and denominator, but the value of time step is different (by about 1% in this example). Thus no extension of the denominator sequence is necessary, and additional unbalanced statistical fluctuations would therefore not occur. The parallel scoring method is expected to be more accurate since the fluctuations in the numerator and denominator are correlated. This is supported by the data of Figure 4 .

In order to compute the energy of a particular configuration of external charges, one may choose the initial state  $|\phi\rangle$  to lie in that particular external charge sector of the Hilbert space. The energy thus computed from equation (1) is automatically the lowest energy eigenvalue in that charge sector. The gap is then given by taking the difference of these lowest statistically independent eigenvalues from sectors corresponding to different length strings. The statistical

fluctuation in computing the gap is obtained by a simple Gaussian propagation of errors. This is the technique employed to generate the data presented in the first row of Table 1.

In Table 1 we compare the energies computed several ways of a unit length string with the vacuum, and a string of length two with a string of length one.

The second method (II) illustrated in the table differs from the first in that energies for the vacuum, unit length string, and two unit string are computed simultaneously as discussed above by using parallel scoring. The final values are then differenced. Thus, while three separate computer jobs are required to generate  $E_0, E_1, E_2$  in the original method, all data in method II is generated by a single computer job requiring only a slightly longer time than that required to compute the single value  $E_0$  via the old method. Note that the values of the new computation of  $E_0, E_1, E_2$  are consistent with original ones. As in the original serial method, the gaps are simply computed by subtracting energies.

The data quoted in the final approach (III) was generated by the parallel score method, so the three E values and their fluctuations are identical to those of Method II. However, the computation of the gaps and their fluctuations is different. In the parallel method (II), the error bars are calculated by dividing the 100,000 data passes into five bins of 20,000 each. The error bar quoted is then the root mean square deviation over the five bins. In Method III, we take advantage of the fact that each bin yields a measurement of all three energies, and simply record the gaps computed in each bin as  $E_1 - E_0$  and  $E_2 - E_1$ . Each of these five bins then yields a measurement of the two gaps. In the third row of Table 1, the quoted number is the mean of the gaps over the five separate bins, and the fluctuation is based on these five independent values. A comparison of

rows 1 and 2 shows that the measurement of the gap by the parallel method has an error bar smaller than the serial method by a factor of 10, even though it was given by a computer calculation one third as long.

We now study the dependence of the gap on the length of the string. In the limit of strong coupling, a string of length  $L$  has energy  $g^2 L$  to leading order, and the tension is  $g^2$ . In Figures 5 and 6 we show the gap versus  $L$  at two different values of the coupling  $g$ . At both values of the coupling, the tension appears to have reached an asymptotic value by  $L$  of one. It is important to note that all data in each of these figures was generated by a single computer job using parallel scoring.

Finally we wish to extract the string tension as a function of coupling. To see how this is done, refer to Figures 5 and 6. Since the string tension appears to have reached an asymptotic value at unit length, we average the tension over all eight measurements. The final quoted error bar is then the average divided by  $\sqrt{n}$ ,  $n = 8$ .

Figure 7 shows the resulting asymptotic string tension for unit external charges as a function of coupling. The strong coupling prediction is also given.

Before proceeding to the conclusion and final discussion, we will compare our results in more detail with that of Potvin and DeGrand (PDG). Figures 8 and 9 include data reproduced from Figure 4 of this reference. Also included on the graph is our data for the same measured quantity produced by a single run using the parallel scoring method. Note that due to differences in the form of the Hamiltonian and in definition of  $g$ , we have translated their parameters to our units by using the relation between couplings  $G^2(PDG) = \sqrt{2}g^2(us)$  and energy densities  $E(us) = \sqrt{2}(E(PDG) - G^{-2})$ . The strong coupling curve is also given

on the figure. Although these results clearly show that parallel scoring produces energies which can be characterized by a string tension, this is not the best way to extract its value. The optimum way is to measure directly the difference  $E(L+1) - E(L)$  for each bin of our data as was done to produce Figures 5 and 6. This procedure is not available using the standard projector method since one cannot measure string tensions in a single run but only the total energy in a given sector.

A further discussion of the detailed differences in the simulations PDG and ourselves will be given in the next section.

## 6. Discussions and Conclusions

In this paper we have presented a new method, parallel scoring, for making measurements in numerical simulations using the stochastic Monte Carlo approach. We have demonstrated that this method not only improves the efficiency but also the accuracy of certain (comparison) measurements, such as energy gaps, string tensions, etc.

In order to further clarify the advantages of parallel scoring, we now turn to a detailed discussion of the differences between the treatment of Potvin and DeGrand (PDG) and that of the present paper. They found that the projector method did not work well, and that the fluctuations in the numerical results were large. Our treatment differs in two important respects. First, we have utilized parallel scoring to improve not only the efficiency but to reduce the statistical fluctuations. Second, the details of the basic formulations of the probabilities and scores are quite different. The major differences are:

1. Our breakup of  $H$  into  $H_1$  and  $H_2$  is symmetric whereas PDG use an unsymmetrical breakup by assigning to each single plaquette Hamiltonian only two of the four possible Electric field operators. This choice does not seem to fully suppress the probability of adding flux to the system.
2. We compute the one plaquette matrix elements essentially exactly, whereas PDG use the lowest order Trotter formula ( $s=1$  in Eqn(25)). Furthermore, we also found that the introduction of the two trial parameters  $g_T$  and  $\Delta_T$  was important in minimizing fluctuations.
3. PDG evaluated some matrix multiplications using the stochastic method which can be done analytically. After breaking up  $e^{-\beta H}$  into a product, and using the symmetric  $s = 1$  Trotter formula on each factor, one obtains adjoining factors of  $e^{(\Delta e/2)} \times e^{(\Delta e/2)}$ . If this product is carried out numerically, extraneous fluctuations are introduced which would not be present in the analytic result  $e^{(\Delta e)}$ .
4. The most important difference in the two calculations is not unrelated to point 2 above. PDG use a probability function which has the same probability for adding  $m$  units of flux as for subtracting  $m$  units. Thus their random walk is not bounded and the electric flux on single links can grow as  $\sqrt{NT}$ . This growth will eventually lead to large fluctuations. Our probabilities are not symmetric and if a plaquette has flux, it will prefer to subtract flux rather than adding more to the system. This feature stabilizes the generation of the random configurations. Furthermore, we see no evidence of an instability at intermediate couplings.

We have found that PQED can be treated by the projector method augmented with parallel scoring. The numerical fluctuations are reasonable and

measurements can be performed quite efficiently<sup>13</sup> down to quite weak coupling.

The application of parallel scoring to three space dimensions will be given in another paper. We expect that our method of measuring the string tension will be sufficiently accurate to clarify the behavior of the transition from strong to weak coupling in this quantity. There are many spin problems which can be attacked by parallel scoring, in this regard see Ref.7, but the particular form of the application depends in detail on the model and the quantity being measured.

#### ACKNOWLEDGEMENTS

We wish to thank David Kung and Robert Sugar for many helpful comments and discussions, and T. DeGrand and J. Potvin for discussions on their work on PQED.

**Table 1**

Typical expectation values and fluctuations of string energies and gaps as measured by methods I, II, III.

	$\underline{E_0}$	$\underline{E_1}$	Gap(1) $\underline{(E_1 - E_0)}$	$\underline{E_2}$	Gap(2) $\underline{(E_2 - E_1)}$
I	$-30.37 \pm 1.44$	$-30.26 \pm 2.20$	$0.11 \pm 2.63$	$-29.84 \pm 1.96$	$0.42 \pm 2.95$
II	$-29.81 \pm 0.60$	$-29.19 \pm 0.65$	$0.62 \pm 0.88$	$-28.71 \pm 0.74$	$0.48 \pm 1.09$
III	"	"	$0.61 \pm 0.14$	"	$0.49 \pm 0.35$

---

$8 \times 8$ lattice;	$20,000 \otimes 5$	Del. = 0.01	$NT = 4$	$DS = 1/4$
$DST/DS = 1.25$	$GT/G = 1.4$	$g = 0.8$		

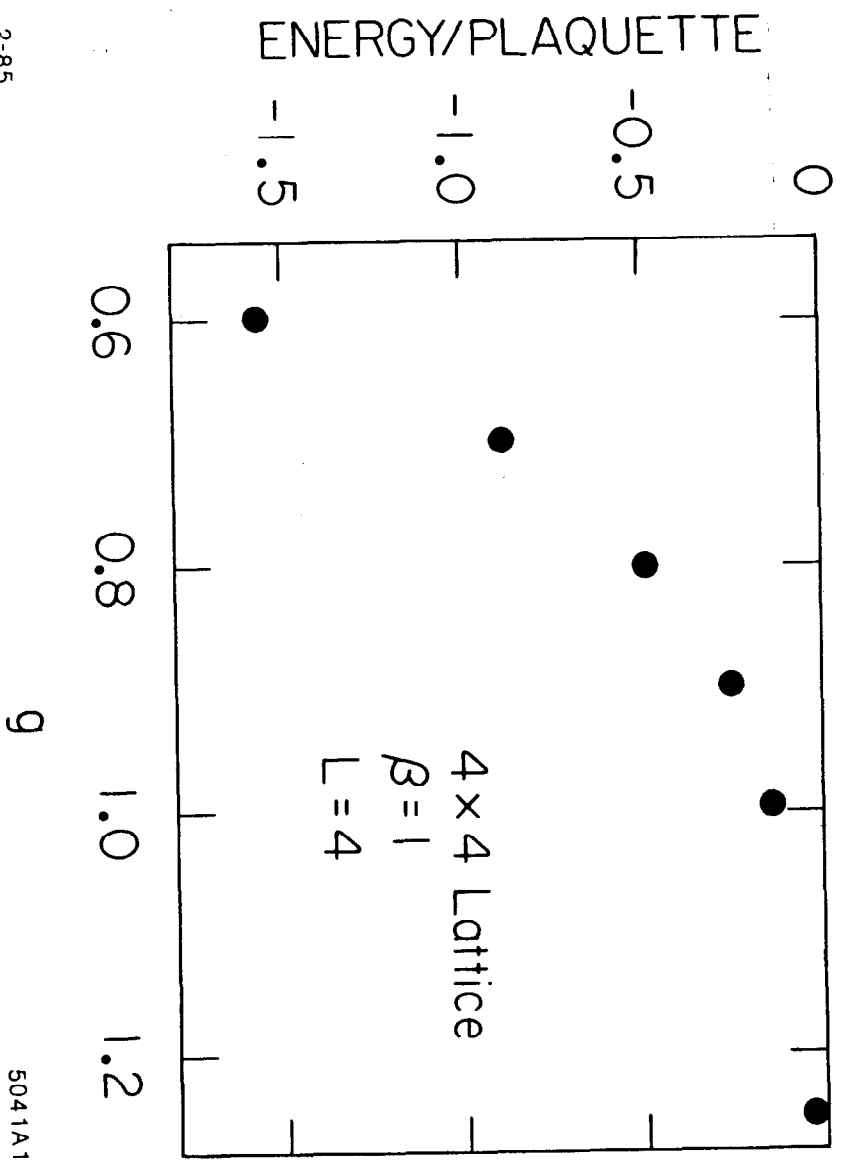
## REFERENCES

1. R. Blankenbecler and R. L. Sugar, Phys. Rev. *D27*, 1304 (1983).
2. See G. E. Forsythe and R. A. Leibler, Math. Tabs. Aids Comput. *4*, 127 (1950). M. Metropolis and S. Ulam, J. Am. Stat. Assoc. *44*, 335 (1949).
3. J. Kuti, Phys. Rev. Lett. *49*, 183 (1982).
4. D. M. Ceperely and M. H. Kalos, in *Monte Carlo Methods in Statistical Physics*, edited by K. Binder (Springer, Berlin, 1979); M. H. Kalos, D. Levesque and L. Verlet, Phys. Rev. *A9*, 2178 (1974).
5. D. M. Ceperely and B. J. Adler, Phys. Rev. Lett. *45*, 560 (1980).
6. Numerical Simulation of Quantum Spin Models, SLAC-PUB-3485, October 1984, D. Kung, R. Blankenbecler, and R. Sugar, submitted to Physical Review B.
7. J. Potvin and T. A. DeGrand, Phys. Rev. *D30*, 1285 (1984). Although these authors used the projector method, it was implemented in a very different way from the calculations in this work. A detailed comparison is made in the conclusion. They are now applying the population or ensemble approach to this problem with more encouraging results.
8. This problem has been studied using the partition function Monte Carlo method by G. Bhanot and M. Creutz, Phys. Rev. *D21*, 2892 (1980). For an analytic approach to this problem, where more references can be found, see H.G. Evertz and D. Horn, Phys. Rev. *D30*, 2664 (1984).
9. J. Hirsch, D. Scalapino, R. Sugar and R. Blankenbecler, Phys. Rev. Lett. *47*, 1628 (1981); Phys. Rev. *B26*, 5033 (1982).

10. A. C. Irving, J. F. Owens and C. J. Hamer, *Phys. Rev. D* **28**, 2059 (1983); A. Hasenfratz, E. Hasenfratz and P. Hasenfratz, *Nucl. Phys. B* **180**, 353 (1981); V. Alessandrini, V. Hakim and A. Krzywicki, *Nucl. Phys. B* **200**[FS4], 355 (1982). A.C. Irving and C.J. Hamer, *Nucl. Phys. B* **235**, 358 (1984).
11. D. W. Heys and D. R. Stump, *Phys. Rev. D* **28**, 2067 (1983).
12. T. Hofsäss and R. Horsley, *Phys. Lett.* **129B**, 65 (1983).
13. All our data presented in this paper were obtained in  $\sim 3$  hours on the SLAC 8 MIPS IBM3081K machine.

## FIGURE CAPTIONS

1. Plot of the energy per plaquette as a function of the coupling  $g$  for the lattice size as given. The statistical errors are roughly one-fourth the size of the dots.
2. Same as Figure 1, but for a larger lattice. The statistical errors are roughly the size of the dots.
3. Same data as Figure 2, presented with the strong coupling calculation shown as the solid line, which becomes dashed when the last term included becomes 1% of the leading term. A few points from a variational calculation are also plotted as diamonds.
4. A comparison of typical statistical fluctuations in the total energy measurement as computed with and without parallel scoring for various size lattices.
5. A plot of the string tension as a function of length for  $g$  in the intermediate region from parallel scoring. All the data points were taken simultaneously.
6. Same as the previous figure but at smaller coupling.
7. A plot of the string tension (averaged over length) as a function of the coupling  $g$ . The result from the strong coupling expansion is also given under conditions described in Fig.3.
8. A comparison of data from ref.(7), plotted as open squares, with data produced using parallel scoring, plotted as closed dots. The strong coupling curve is also given.
9. Same graph as Fig.8 but at weaker coupling. The strong coupling expansion completely fails at this value of  $g$ .



2-85

5041A1

Fig. 1

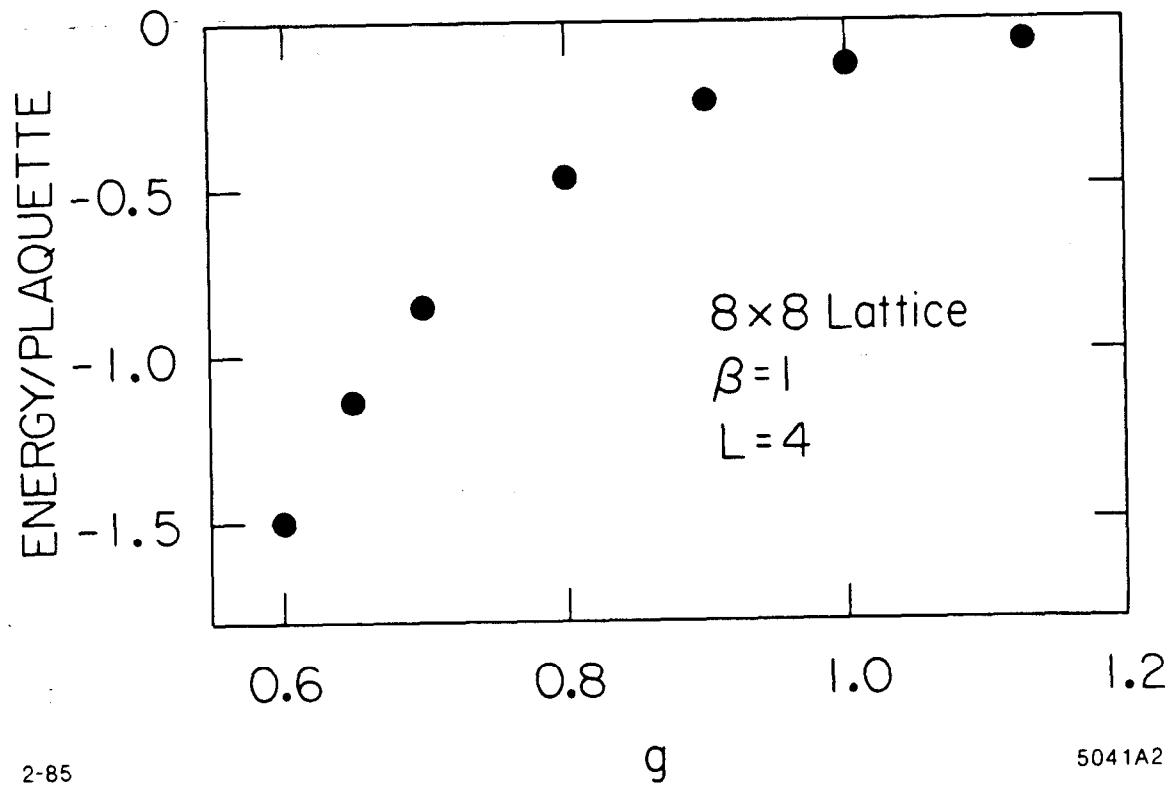
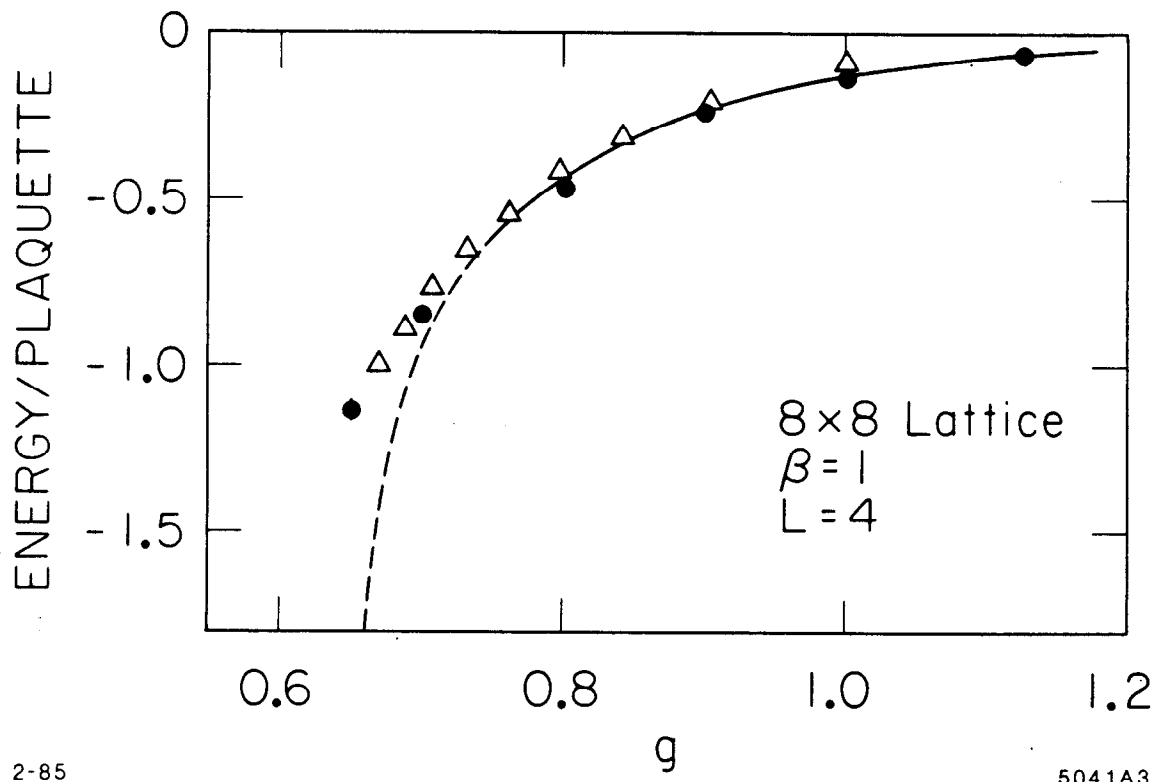


Fig. 2



2-85

5041A3

Fig. 3

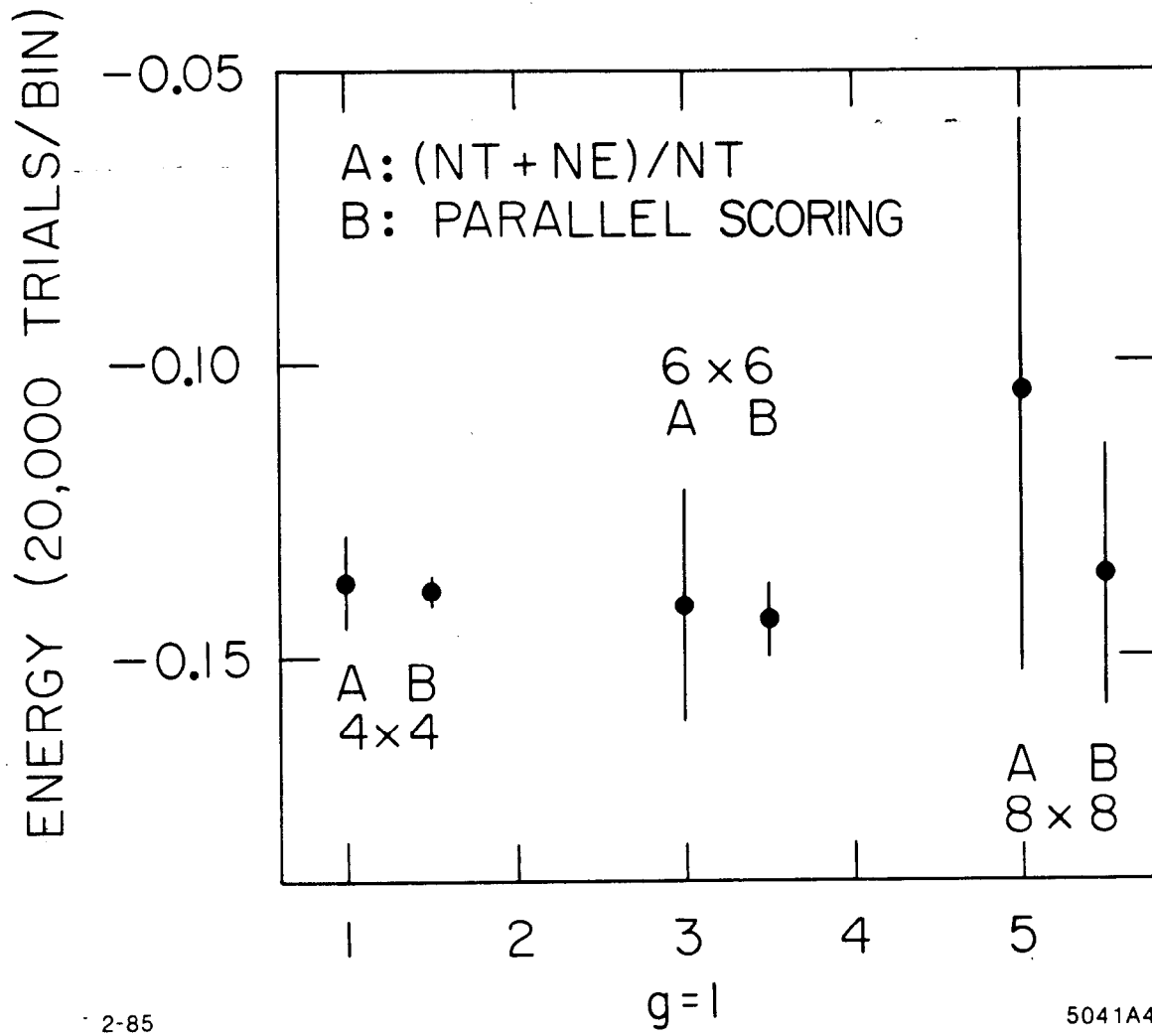


Fig. 4

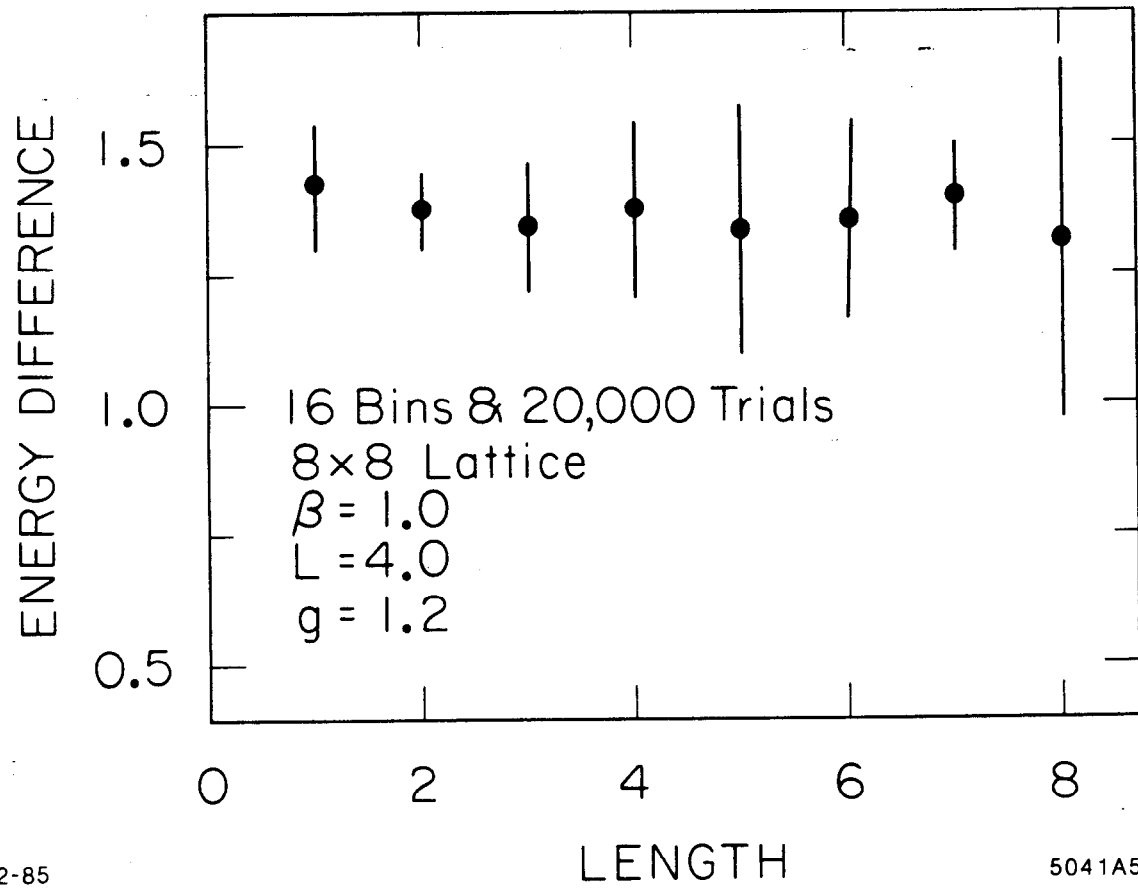
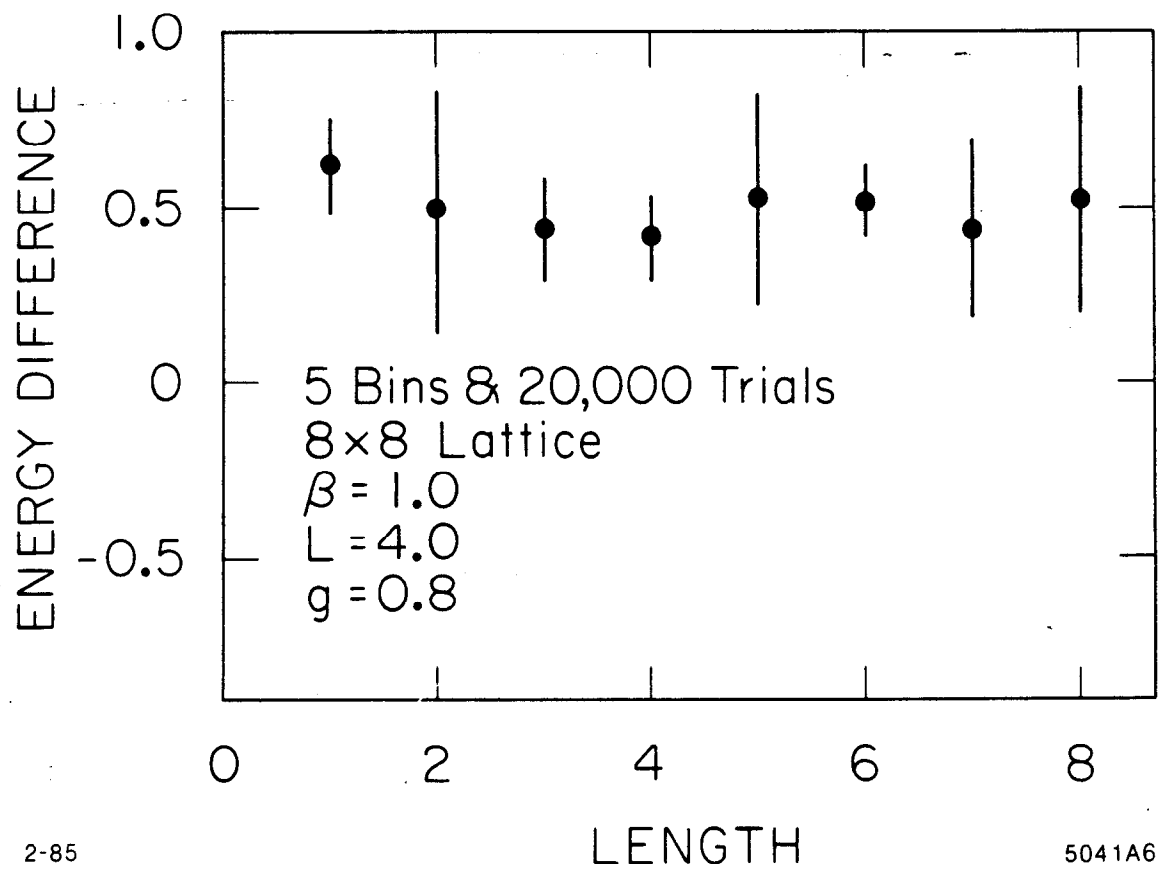


Fig. 5



2-85

5041A6

Fig. 6

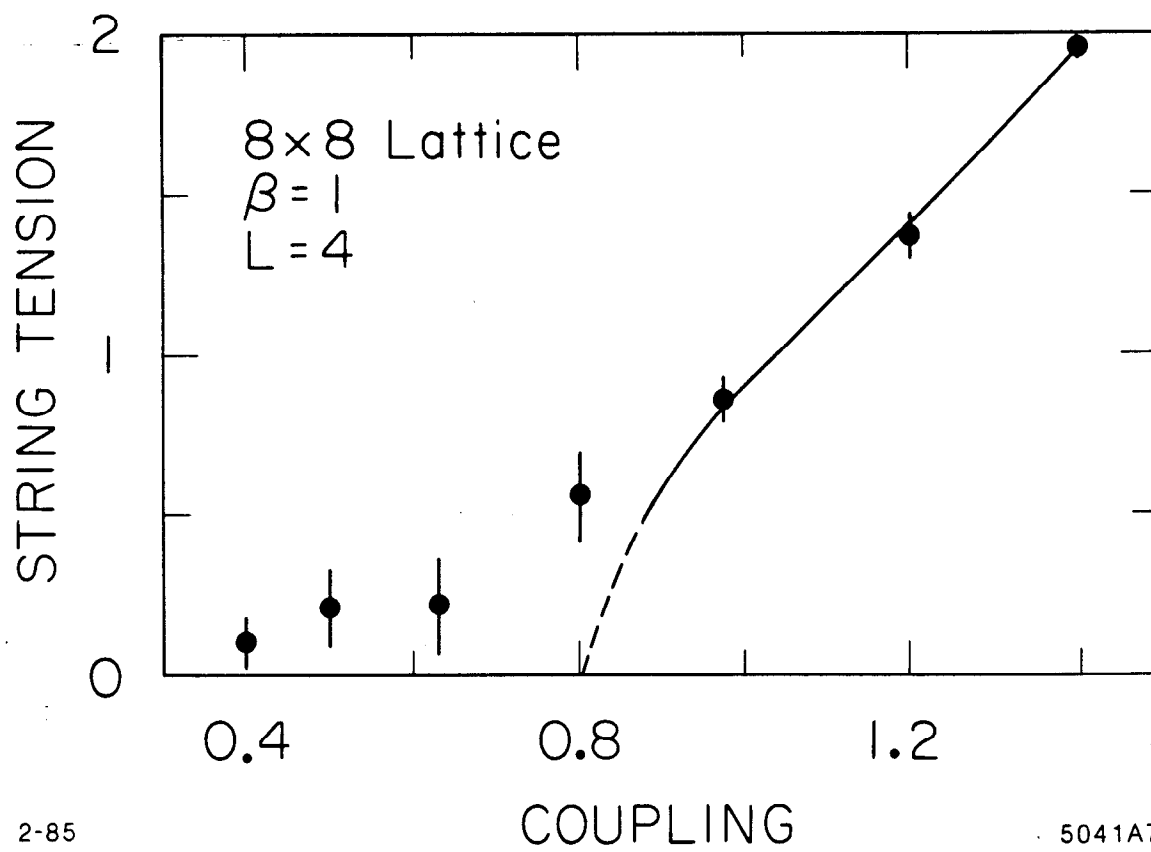


Fig. 7

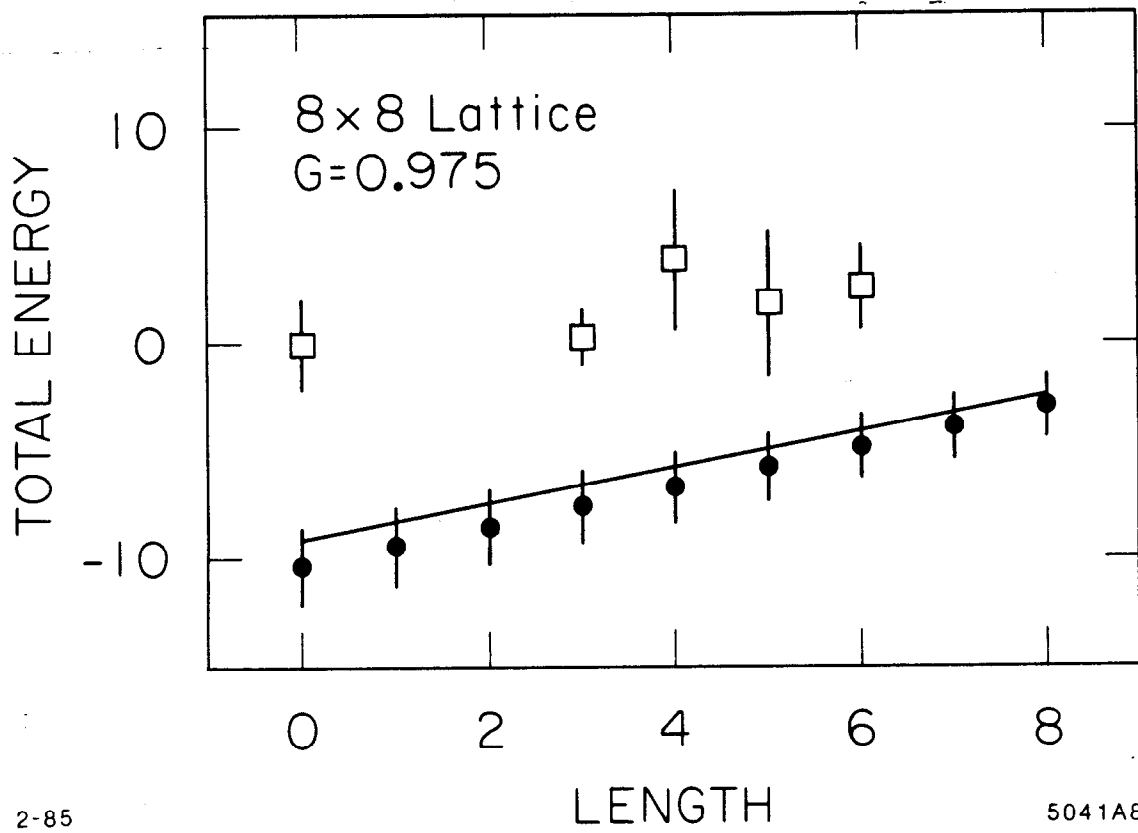


Fig. 8

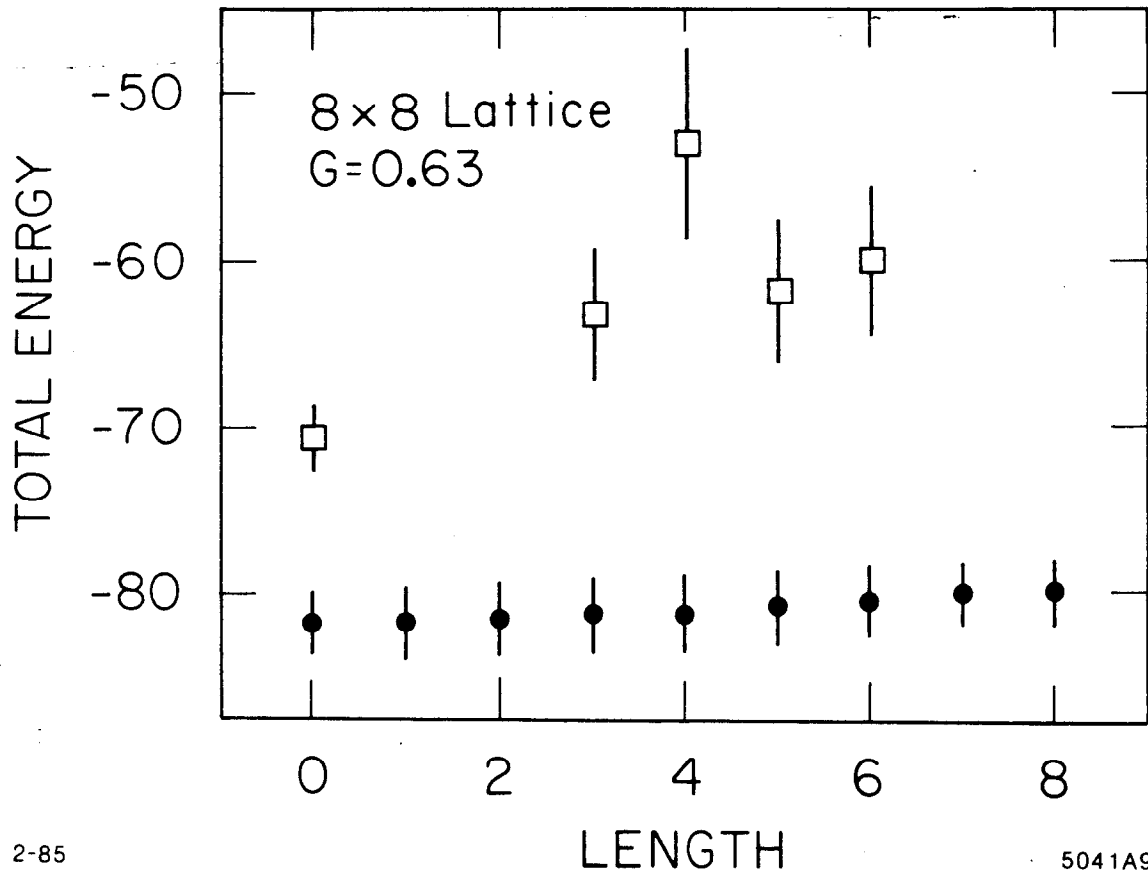


Fig. 9